HHS Public Access

Author manuscript

Phys Med Biol. Author manuscript; available in PMC 2020 April 30.

Published in final edited form as:

Phys Med Biol. ; 65(9): 095004. doi:10.1088/1361-6560/ab7d16.

Tracking tumor radiotherapy response *in vivo* with Cherenkov-excited luminescence ink imaging

Jennifer A. Soter[1], **Ethan P. M. LaRochelle**[1], **Brook K. Byrd**[1], **Irwin I. Tendler**[1], **Jason R. Gunn**[1], **Boyu Meng**[1], **Rendy R. Strawbridge**[1], **Dennis J. Wirth**[1], **Scott C. Davis**[1], **David J. Gladstone**[1,3], **Lesley A. Jarvis**[3], **Brian W. Pogue**[1,2,*]

[1]Thayer School of Engineering at Dartmouth, Hanover, NH 03755, USA

[2]DoseOptics LLC, Lebanon, NH 03766, USA

[3]Geisel School of Medicine at Dartmouth, Hanover, NH 03755, USA

Abstract

Purpose: This study demonstrates remote imaging for *in vivo* detection of radiation-induced tumor microstructural changes by tracking the diffusive spread of injected intratumor UV excited tattoo ink using Cherenkov-excited luminescence imaging (CELI).

Methods: Micro-liter quantities of luminescent tattoo ink with UV absorption and visible emission were injected at a depth of 2mm into mouse tumors prior to receiving a high dose treatment of radiation. X-rays from a clinical linear accelerator were used to excite phosphorescent compounds within the tattoo ink through Cherenkov emission. The *in vivo* phosphorescence was detected using a time-gated intensified CMOS camera immediately after injection, and then again at varying time points after the ink had broken down with the apoptotic tumor cells. *ex vivo* tumors were imaged post-mortem using hyperspectral cryo-fluorescence imaging to quantify necrosis and compared to Cherenkov-excited light imaging of diffusive ink spread measured *in vivo*.

Results: Imaging of untreated control mice showed that ink distributions remained constant after four days with less than 3% diffusive spread measured using full width at 20% max. For all mice, *in vivo* CELI measurements matched within 12% of the values estimated by the high-resolution *ex vivo* sliced luminescence imaging of the tumors. The tattoo ink spread in treated mice was found to correlate well with the nonperfusion necrotic core volume (R^2=0.92) but not well with total tumor volume changes (R^2=0.34).

Conclusion: *In vivo* and *ex vivo* findings indicate that the diffusive spread of the injected tattoo ink can be related to radiation-induced necrosis, independent of total tumor volume change. Tracking the diffusive spread of the ink allows for distinguishing between an increase in tumor size due to new cellular growth and an increase in tumor size due to edema. Furthermore, the imaging resolution of CELI allows for *in vivo* tracking of subtle microenvironmental changes which occur earlier than tumor shrinkage and this offers the potential for novel, minimally invasive radiotherapy response assay without interrupting a singular clinical workflow.

*Corresponding author: brian.w.pogue@dartmouth.edu.

Conflict of Interest Statement: B. Pogue is president and co-founder of DoseOptics LLC, who supplied the camera used in this research. S. Davis has a financial interest (Member) in DoseOptics, LLC.

Introduction

Most techniques for tracking treatment progression in radiation therapy are anatomically based, measuring the size of the tumor through exams such as a weekly computed tomography (CT) scan[1–4]. These can fail to detect subtle changes in tumor response at the cellular level that could provide useful insight, especially for combination therapies utilizing radiation[4]. Therefore, there has been a recent emphasis towards functional imaging since it is widely recognized that changes to the tumor microenvironment including hypoxia and angiogenesis are strong indicators of treatment response[5,6]. A number of functional imaging modalities are capable of characterizing biological processes that can better assess tumor microenvironmental responses and allow for the development of personalized treatment[1–4,7]. While many of these modalities show reasonable fidelity for tumor change in metabolism or function, they all require the logistical challenge of an additional imaging procedure, which was the motivation for the work in this study.

The information gained in positron emission tomography (PET), for example, can observe tumor properties such as cell metabolic activity and hypoxia with the use of radiotracers like ^{18}F-fluoro-deoxyglucose[8]. Perhaps the closest imaging technology to this work is diffusion-weighted magnetic resonance imaging (MRI), which can quantify the rate of microscopic water diffusion *in vivo* and is a promising technique for radiation response evaluation since cell membrane integrity is part of what is imaged here[9,10]. Extrinsic contrast agents can additionally be utilized to quantify tumor blood flow and other cellular processes, such as used dynamic contrast-enhanced (DCE) imaging MRI, DCE or perfusion CT, and DCE ultrasound imaging (DCE-US), but each of these measure intravenous agent contrast and leakage and so are more related to vascular damage then tumor parenchyma damage[1–3,11].

PET, MRI, and CT scans ultimately all have limited spatial resolution and are timely, expensive procedures that require a separate scheduled exam in the medical center[1,4,6]. Thus, these techniques are commonly performed at most on a weekly or monthly basis to assess tumor response[4]. DCE-US, though low-cost, readily available and non-ionizing, offers low spatial resolution in comparison and is mostly limited to imaging abdominal or superficial organs[1,12]. Therefore, the ability to image tumor microenvironment changes on a daily basis for patient management feedback during a radiation treatment without interrupting clinical workflow would be advantageous in treatment management.

A handful of recent reports focused on functional imaging techniques for treatment response assessment to chemotherapy agents have described the use of intra-tumoral injections of fluorescent dyes to track immune response changes using *ex vivo* microscopy[13–15]. Therefore, to address the issue in radiation therapy, a novel method to measure radiation-induced tumor response *in vivo* was examined here using intra-tumoral injections of a luminescent tattoo ink. The hypothesis was that a diffusive spreading of the luminescent dye could be related to the breakdown of tumor cells in response to radiation and, using Cherenkov-excited luminescence imaging techniques[16–18] this diffusive spread could be measured *in vivo* during radiotherapy with little more than addition of a camera to the room.

Cherenkov-excited luminescence imaging (CELI) techniques are based on the concept that an intensified camera can be synchronized with the 4μs-long radiation pulses that are delivered every 2.8ms from a clinical linear accelerator, and can record only the luminescent signals between each pulse[16–18]. When the beam is on, Cherenkov light is generated in biological tissue with intensity of 10^8-10^{10} optical photons for each X-ray photon entering from a therapeutic MV beam as a result of secondary scattered electrons[17]. With an emission spectra weighted towards ultraviolet and blue frequencies but continuing throughout the visible and NIR range, this Cherenkov light acts as an internal excitation source for luminescent agents[16]. Thus, the delayed, secondary, low signal phosphorescence can be imaged during the absence of high intensity Cherenkov light by time gating to when the beam is off. The major advantage in CELI is the ability to achieve tissue excitation with the use of MV X-rays that penetrate deeper than any other whole-body optical molecular imaging system, making CELI techniques a potential tool for imaging intratumoral molecular diffusion with an optimized luminescent marker.

The goal of this work was to evaluate the feasibility and potential for using CELI in a mouse model to directly track subtle tumor microenvironmental changes in response to radiation therapy. In this study, UV-sensitive phosphorescent tattoo ink was used as the intratumoral luminescent marking agent and Cherenkov light was generated in the tissue using MV X-ray radiation beams. CELI was examined for measurement of the daily spread of ink diffusion in murine tumors treated with a high dose single fraction radiation. This was correlated to the amount of induced necrotic tissue using post-mortem hyperspectral cryo-fluorescence imaging to track treatment response more reliably than tumor volume measurements.

Materials and Methods

Phosphorescent ink

UV-sensitive tattoo ink (Mom’s Nuclear Inks LLC, USA) that is used in human tattooing, was used as the luminescent marker. Although tattoos are generally administered through intradermal injections of an ink, tattoo inks are considered cosmetic products and not regulated by the Food and Drug Administration[19]. Therefore, recorded assessments of the chemical composition of these inks are unavailable and the formulation remains proprietary. However, the optical properties of these UV-sensitive tattoo inks were investigated in previous work and shown to have a broad absorption spectrum in the UV/blue range and emit phosphorescence in the visible range with microsecond lifetimes. The color “Afterglow Yellow” was selected for this work as this color was reported to emit the highest signal intensity in prior Cherenkov-excitation phantom imaging studies (LaRochelle *et al* 2020). The luminescent lifetime was reported to be 15.5 ±1.8μs. The ink was also measured to have a peak emission wavelength at 505nm, but with a very broad emission bandwidth that extends out to beyond 660nm. While much of the green and yellow wavelengths of this emission are absorbed by blood, the red wavelengths 600–660nm are readily passed through soft tissue.

Tumor cells and animal preparation

Cells from the radio-responsive human head and neck cancer cell line A431 (ATCC, Manassas Virginia) were used to grow tumors in mice. Specifications on the cell inoculation protocol has been described in previous work[1]. All animal procedures were approved by the Dartmouth Institutional Animal Care and Use Committee and all procedures followed the approved protocol. The *in vivo* CELSI animal experiments have been previously described[17]. For this work, twenty athymic nude female mice were purchased at 6 weeks of age from Charles River Labs. Animals were given a week of acclimatization prior to injections of 10^6 cells subcutaneously on the right flank in individual 0.050mL injections. Mice were selected for the imaging study after approximately 10 days of growth, once the tumor reached between 150–250mm^3 in volume. All mice were placed under general anesthesia using 3% isoflurane mixed with pure oxygen via a nose cone throughout injections, treatment, Cherenkov-excited luminescence imaging procedures, and euthanasia following the final CEL imaging.

Intratumoral luminescent injections

Anesthetized mice, positioned on a custom stereotactic injection platform and immobilized with medical tape, were injected with 0.015mL of undiluted yellow tattoo ink into the center of the tumor, 2mm orthogonally under the surface of the skin as seen in Figure 1b. All eighteen mice received an intratumoral injection of the phosphorescent ink. The injections were performed using a 27-gauge needle secured within a stereotaxic platform to ensure depth accuracy and directional consistency. Mice remained anesthetized on the custom platform while they were transferred to the linear accelerator treatment couch immediately after injection for the initial image acquisition. After aligning the mouse and preparing the linac bunker, the first images were acquired approximately 10–15 minutes after the dye was injected.

In vivo imaging setup

A static 6MV photon beam delivered by a Varian Linac 2100C (Varian Medical Systems, Palo Alto, CA) was used irradiate all tissue samples and intended to mimic a typical 2Gy radiotherapy fraction. The beam geometry used for all *in vivo* measurements was setup to irradiate the mouse from below with a 100×100mm^2 field size delivering 200MU at a rate of 600MU/min, which equates to a whole-body dose of 2Gy for the mouse. The 6MV photon beam was delivered by the linac in 4μs-long pulses at a repetition rate of 360Hz.

Delayed phosphorescence was detected using a time-gated intensified CMOS camera, C-Dose (DoseOptics LLC, NH, USA) coupled to a Nikkor 50-mm f/1.2 AF lens (Nikon Corporation, Tokyo, Japan) positioned approximately 1.5 meters away with the mouse aligned at isocenter. No optical filters were used to limit spectral bandwidth of the camera, however the photocathode sensitivity of the camera was weighted toward the red optical wavelengths. The wavelength-dependent sensitivity of this camera has been published in a previous study[20]. Specifications on the image acquisition and camera output workflow have also been described previously[21,22]. For this work, images were acquired with a 5μs time-delay after each pulse of the 6MV photon beam for a duration of 150μs (10 times the lifetime of the phosphorescent dye) over a 50ms CMOS exposure time. Approximately 370

frames were acquired during one 200MU CEL imaging session. All measurements were recorded with the imaging apparatus covered under blackout curtains. A detailed schematic of the imaging setup is illustrated in Figure 1a.

Images were processed offline using ImageJ (National Health Institute, USA). The images were background subtracted, darkfield and flatfield corrected and a spatial (4 × 4-pixel window size) median filter was applied to increase signal-to-noise ratio. A fast Fourier transform bandpass filter was also applied using an ImageJ plugin to suppress vertical strips due to background (with a 5% tolerance), filter large objects down to 40 pixels and small structures up to 4 pixels. MATLAB (MathWorks, Natick, MA) was used for additional image analysis.

Imaging & treatment workflow

To demonstrate the potential of using CELI in conjunction with the radiation delivered during a typical 2Gy treatment fraction to track tumor response, a 2Gy treatment fraction was delivered (immediately after the phosphorescent ink was injected) and the initial CELI session was performed simultaneously to measure the initial baseline spread of the ink. To illicit a stark difference in radiation response, one group of mice (n=15), received an additional treatment of 10Gy localized to the surface of the right flank at a dose rate of 600MU/min using a 6MeV electron beam and a $60\times60mm^2$ electron applicator (Varian Medical Systems, Palo Alto, CA) following the initial CELI measurement. The remaining untreated control mice (n=5) received no additional radiation after the first CELI acquisition on Day 0.

A second 2Gy treatment fraction was delivered for all mice one to six days later so that a second, final CELI session could be performed simultaneously to observe the relative change in ink spread from Day 0. Mice were euthanized immediately after the final image for *ex vivo* analysis. A workflow chart summarizing the *in vivo* procedure/measurement time points for all mice is presented in Figure 2 and Table 1. Immediately after euthanasia, the tumor volume was harvested from the mouse, embedded in clear Tissue Plus® Optimal Cutting Temperature medium (Fisher HealthCare, Houston, TX) inside a plastic cryomold, then snap-freezing using solid carbon dioxide. The procedure used for snap-freezing the tumor samples as reported elsewhere.

Ex vivo cryo-fluorescence imaging

The imaging cryo-macrotome system consisted of a refurbished Leica CM3600 whole body Cryomacrocut modified with a custom control system and advanced multi-channel fluorescence imaging module. This instrument automatically images frozen blocks of tissue specimens during sectioning, producing high-resolution 3-D volumes of RGB color images and fluorophore distribution throughout the entire specimen. The imaging module was positioned 40cm above the sample and consisted of a bank of LED and laser sources for illumination, accompanied by a high-speed filter wheel (HS1024, FLI, Lima, NY), liquid crystal tunable file (LCTF, VariSpect, PerkinElmer, Waltham, MA) and scientific CMOS cameras (PCO Edge 4.2 s, Kelheim, Germany) for imaging the remitted light.

In this study, we acquired brightfield RGB data and emission images of the phosphorescent ink. The former was acquired by illuminating with a broadband white LED (Mightex, Toronto, ON) and acquiring reflectance images at discrete wavelengths using the LCTF (420nm to 720nm in steps of 10 nm). Phosphorescence images were acquired by illuminating with a 470nm LED (Mightex, Toronto, ON) fitted with a 475nm short pass filter (ThorLabs, Newton, NJ) and acquiring emission images using a 500nm dichroic long pass filter (ThorsLabs, Newton, NJ) and LCTF set to 560nm, The spatial resolution for each image was 100μm or better and specimens were sectioned at 100μm thickness, resulting in a voxel resolution of 100μm in all dimensions. The fully automated data collection sequence was as follows: Acquire white light reflectance images at each LCTF wavelength, acquire ink phosphorescence image (470nm excitation), cut section and repeat imaging. Sectioning at 100μm resulted in about 100–200 cuts per specimen. In most cases, four specimens were cryo-imaged simultaneously.

Each image was corrected for dark current, flat-field inhomogeneities, radial distortion and exposure time. After corrections were applied, the hyperspectral white light image stacks were remixed through spectral weighting to produce RGB color images using the CIE XYZ tristimulus mapping algorithm reported elsewhere[24]. Color images and volumetric rendering of the phosphorescent ink were visualized and analyzed using ImageJ (National Health Institute, USA). A color detection algorithm described previously was implemented in MATLAB (MathWorks, Natick, MA) based on the reflectance spectra from regions of interest on the tumor slice to render the non-perfusing necrotic core volume of the tumor[25]. With a color ratio detector to highlight the darker non-perfused tissue region that is weighted stronger toward the red channel, the fraction of necrotic core was calculated across all RGB slices.

Statistical Analysis

Group averages were analyzed using a small-sample Student's t-test to assess the validity of the differences between two means. A p value <0.005 was used as a cutoff for statistical significance. Least squares curve fitting to determine correlation was performed using the scaled Levenberg-Marquardt algorithm with 1000 iterations and a tolerance of 10^{-5}. All statistical analyses were performed with QtiPlot software (Vasilief, Bucuresti, Romania).

Results

In vivo imaging studies

Example Cherenkov-excited images of the ink acquired *in vivo* on Day 0 (immediately after injection) are compared to the final diffusive ink spread (imaged immediately before sacrificing) in Figure 3a,b for treated and control mice. The relative diffusive spread is determined by calculating the relative change in full width at 20% max of the profile intensity plot between the reference Day 0 acquisition and the final acquisition. The example mice in Figure 3a,b show a 29% diffusive spread in the treated tumor after one day and 79% spread four days post treatment; the matching untreated tumors measured 4.2% and 6.1% respectively.

Boxplots summarizing the relative change in diffusive spread measured in all untreated control and treated mice are shown in Figure 3c, where mice are grouped by day post-treatment. Mean value in relative diffusive spread seen among the control group was found to be 0.17 ±0.03 (mean ±std) and by six days post injection, the mean diffusive spread in treated mice reached 1.3 ±0.1 (mean ±std). A significant difference ($p<0.002$, two-sample Student's t test) in the mean diffusive spread values was seen starting two days post injection between the treated mice (0.53 ±0.13, mean ±std) and the control mice (0.17 ±0.03, mean ±std). No difference was seen in data collected from mice euthanized after one day.

Ex vivo imaging studies

Several example RGB image slices are presented in Figure 4a for treated mouse euthanized and snap-frozen for *ex vivo* imaging. Reflectance spectra from various regions of interest (ROI) are also displayed in Figure 3a and were selected to represent three different structures in the tumor – the non-perfusing necrotic core, the viable tissue, and the tattoo dye (outlined in black, pink, and yellow respectively). A color detection algorithm described previously (cite) was implemented based on the reflectance spectra from these ROIs to render the non-perfusing necrotic core volume of the tumor. With a color ratio detector to highlight the darker tissue region that is weighted stronger toward the red channel, the fraction of necrotic core was calculated across all RGB slices; Figure 4b shows examples of the results of this algorithm.

As the fraction of non-perfusing core to total tumor volume increases, the representative fluorescence image slices and corresponding *in vivo* CELI measurements show increasing ink diffusion. Box plots of the necrotic core fraction for all treated and control mice are organized by day post initial CELI in Figure 5c. The total tumor volume measurements, measured manually with calipers, is also presented to the left.

The fraction of non-perfusing necrotic core for each tumor, as opposed to total volume measurements, provides a more useful response metric to explain the trends in ink breakdown (Figure 5d). An analysis of the diffusive spread *in vivo* measurements with all individual mouse data points showed a strong correlation ($R^2=0.92$) with percentage of necrotic volume, but a weak correlation with tumor volume ($R^2=0.34$).

Maximum intensity projections to visualize the entire ink volume in 3-dimensions are shown in video format in the Supplementary Material for these tumors.

The higher resolution *ex vivo* data obtained with the cryo-fluorescence imaging supports the trends seen during the *in vivo* experiments. Z-projections for each of the stacks of *ex vivo* fluorescence images were generated in ImageJ (National Institute of Health, USA) to compare more directly with the *in vivo* experimental setup. Example Z-projections for responsive and control tumors one, two and four days post injection are presented with the corresponding *ex vivo* profile spreads (Figure 5a,b). The average full width at 20% max was also found to be significantly different ($P<0.005$) between the control mice (6.02 ±1.1mm, mean ±std) and the treated mice (12.7 ±1.6mm, mean ±std). Furthermore, these *ex vivo* estimates of the ink volume diffusion based on the full width at 20% max of the lateral

spread of the z-projection were found to linearly correlate with the Cherenkov estimates measured *in vivo* (R^2=0.93).

Discussion

Both *in vivo* and *ex vivo* analysis revealed that the tumor line responded to the single high dose fraction of radiation. A 10 Gy dose was chosen based on an earlier study characterizing the radiation sensitivity of human squamous carcinoma A431 cells[26]. The use of *in vivo* CELI to track the diffusive spread of phosphorescent tattoo ink as a measure of treatment response in an A431 mouse xenograft model was successful after two days. Changes in the full width at 20% max of the ink spread profiles were measured *in vivo* with widefield imaging up to six days following a single high dose treatment fraction; statistically significant differences ($P < 0.002$) were seen daily with the untreated mice starting two days post-treatment.

Ex vivo analysis techniques confirmed these trends seen with *in vivo* Cherenkov-excited imaging. Although the tumors contain small, non-perfusing central cores of necrosis prior to radiation treatment, the large time-dependent increase in non-perfusion volume observed in the *ex vivo* RGB cryo-images suggests that persistent radiation-induced necrosis was triggered in the treated mice to cause ink spreading. The overall increase in total tumor volume measured in the treated group during days 1–4 post treatment was likely due to an acute inflammatory response typical of radiation-induced necrosis following a single high dose fraction and has been reported in other studies[15–18]. Despite increasing non-perfusion tumor tissue beginning one day after treatment, a decrease in total tumor volume was not observed until day six. Thus, the non-perfusion necrotic core volume, as opposed to the total anatomical tumor volume measurements, was a more valuable metric of treatment response to match with the ink diffusion measurements. *In vivo* measurements of the ink profile spread from Cherenkov-excitation were found to strongly correlate (R^2=0.92) with the percentage of necrotic tumor volume determined *ex vivo*, whereas tumor volume measurements correlated poorly (R^2=0.34).

Analysis of the ink profile spread measured using *ex vivo* cryo-fluorescence imaging supports the profile estimates obtained with Cherenkov-excitation and suggests the proposed *in vivo* imaging system has the potential to track treatment response daily. A strong linear correlation (R^2=0.93) was found between the *in vivo* and *ex vivo* ink profile spreads at full width at 20% max with an average percent difference of 12% (n=15). Though a moderate percent difference was seen, the current *in vivo* set up using widefield irradiation to image the ink spread has substantial room for improvement.

Sheet-scanning illumination would likely offer higher resolution and lower percent differences between the *in vivo* Cherenkov measurements and *ex vivo* cryo-fluorescence imaging. Previous studies report Cherenkov-excited luminesce scanning imaging (CELSI) can achieve spatial resolution of 100–300μm at 3–4mm of tissue depth under blackout conditions[17,22]. Ultimately, development beyond the addition of sheet-scanning, such as the implementation of optical filters or a denoising neural network to increase SNR or multi-

camera imaging for background correction, would be needed for clinical translatability of this work.

Translatability to a clinical setting would also require development focused on the phosphorescent tattoo ink. The ink used in this study had spectral properties that made a suitable Cherenkov-excited luminescent marker to test in a mouse model, but has the ink not undergone safety evaluation for use in humans and its exact composition is unknown. Tattoo ink in general raises toxicity concerns within the medical community and two studies have reported complications due to UV-sensitive tattoo ink in particular[30,31]. A previous study has investigated cellular effects due to the chemical properties changes in tattoo inks after repeated irradiation[32]. Therefore, a complete chemical analysis of the ink and its cellular effects may be needed in the future.

Future experiments looking at the effects of injection site would also need to be performed to determine ways to account for the inherent heterogeneity in the tumor tissue structure. Since tumor perfusion is not uniform, and it is generally believed that the necrotic, non-perfused zone of the tumor grows outward starting from the tumor core, the amount of ink diffusion is expected to vary if the injection site is chosen closer to the tumor's outside perimeter as opposed to its core. As a preliminary proof of concept, we attempted to maintain injection consistency in the center of the tumor and did not yet look into the effects of injection site decision. However, this is a certainly a factor to investigate for future work and we hypothesize a potential solution to better account for tumor structure heterogeneity would be to track multiple small injections located at varying sites throughout the tumor volume.

Lastly to note, long-term future development of the phosphorescent tattoo ink could utilize CELI beyond a radiotherapy assay. Similar to the Comparative In Vivo Oncology (CIVO) arrayed microinjection platform, the ink could potentially be coupled to chemotherapeutic agents for multiple simultaneous intra-tumoral injections to act as an *in vivo* immunological assay measuring tumor responsiveness. But compared to the CIVO platform, CELI does not require autoradiography of *ex vivo* cryo-sections and would able to generate similar information useful to cancer drug development in real time with a minimally invasive imaging technique.

Conclusion

Results indicate the diffusive spreading of the injected tattoo ink can be related to radiation-induced necrosis. *Ex vivo* fluorescence slice-imaging confirmed ink profile spread imaged *in vivo* with widefield irradiation, although the use of sheet-scanning illumination would have provided higher resolution images. Nonperfusion necrotic core volumes determined with *ex vivo* image analysis related to the *in vivo* CELI measurements, however, the use of MRI or H&E to determine the total nonperfusion volume information would be a more reliable assessment. In summary, we have presented a proof-of-concept for a novel, *in vivo* radiotherapy response assay using CELI to measure daily tumor microenvironmental changes at a vascular level without interrupting clinical workflow. With further development,

the approach could have potential applications in personalized drug development and immunological assessments to significantly improve treatment management.

Acknowledgements

This work has been supported by NIH research grants R01 EB024498, R01 CA184354, and R01 CA188491 and use of the shared irradiation facilities at the Norris Cotton Cancer Center, supported by grant P30 CA023108.

Sources of Support: NIH grants R01 EB024498, P30 CA023108, R01 CA184354, R01 CA188491.

References

1. Marcus CD et al. Imaging techniques to evaluate the response to treatment in oncology: Current standards and perspectives. Crit. Rev. Oncol. Hematol 72, 217–238 (2009). [PubMed: 18760935]
2. Rafat M, Ali R & Graves EE Imaging radiation response in tumor and normal tissue. Am. J. Nucl. Med. Mol. Imaging 5, 317–332 (2015). [PubMed: 26269771]
3. Padhani AR & Miles KA Multiparametric Imaging of Tumor Response to Therapy. Radiology 256, 348–364 (2010). [PubMed: 20656830]
4. Bhatnagar P, Subesinghe M, Patel C, Prestwich R & Scarsbrook AF Functional Imaging for Radiation Treatment Planning, Response Assessment, and Adaptive Therapy in Head and Neck Cancer. RadioGraphics 33, 1909–1929 (2013). [PubMed: 24224586]
5. Colliez F, Gallez B & Jordan BF Assessing Tumor Oxygenation for Predicting Outcome in Radiation Oncology: A Review of Studies Correlating Tumor Hypoxic Status and Outcome in the Preclinical and Clinical Settings. Front. Oncol 7, 10 (2017). [PubMed: 28180110]
6. Gwyther SJ Current standards for response evaluation by imaging techniques. Eur. J. Nucl. Med. Mol. Imaging 33, 11–15 (2006). [PubMed: 16783564]
7. Zhou Z & Lu Z-R Molecular imaging of the tumor microenvironment. Adv. Drug Deliv. Rev 113, 24–48 (2017). [PubMed: 27497513]
8. Zhu A, Marcus DM, Shu H-KG & Shim H Application of Metabolic PET Imaging in Radiation Oncology. Radiat. Res 177, 436–448 (2012). [PubMed: 22339451]
9. Hamstra DA, Rehemtulla A & Ross BD Diffusion Magnetic Resonance Imaging: A Biomarker for Treatment Response in Oncology. J. Clin. Oncol 25, 4104–4109 (2007). [PubMed: 17827460]
10. Galbán CJ, Hoff BA, Chenevert TL & Ross BD Diffusion MRI in early cancer therapeutic response assessment. NMR Biomed. 30, (2017).
11. Gaddikeri S, Gaddikeri RS, Tailor T & Anzai Y Dynamic Contrast-Enhanced MR Imaging in Head and Neck Cancer: Techniques and Clinical Applications. Am. J. Neuroradiol 37, 588–595 (2016). [PubMed: 26427839]
12. Leen E et al. Dynamic contrast enhanced ultrasound assessment of the vascular effects of novel therapeutics in early stage trials. Eur. Radiol 22, 1442–1450 (2012). [PubMed: 22302501]
13. Klinghoffer RA et al. A technology platform to assess multiple cancer agents simultaneously within a patient's tumor. Sci. Transl. Med 7, 284ra58 (2015).
14. Dey J et al. A Platform for Rapid, Quantitative Assessment of Multiple Drug Combinations Simultaneously in Solid Tumors In Vivo. PLoS ONE 11, (2016).
15. Frazier JP et al. Multidrug Analyses in Patients Distinguish Efficacious Cancer Agents Based on Both Tumor Cell Killing and Immunomodulation. Cancer Res. 77, 2869–2880 (2017). [PubMed: 28364003]
16. Zhang R et al. Cherenkov-excited luminescence scanned imaging. Opt. Lett 40, 827–830 (2015). [PubMed: 25723443]
17. Pogue BW et al. Maps of in vivo oxygen pressure with submillimetre resolution and nanomolar sensitivity enabled by Cherenkov-excited luminescence scanned imaging. Nat. Biomed. Eng 2, 254–264 (2018). [PubMed: 30899599]

18. Jia MJ, Bruza P, Jarvis LA, Gladstone DJ & Pogue BW Multi-beam scan analysis with a clinical LINAC for high resolution Cherenkov-excited molecular luminescence imaging in tissue. Biomed. Opt. Express 9, 4217–4234 (2018). [PubMed: 30615721]
19. Maarouf M, Saberian C, Segal RJ & Shi VY A New Era For Tattoos, with New Potential Complications. J. Clin. Aesthetic Dermatol 12, 37–38 (2019).
20. Alexander DA et al. Assessment of imaging Cherenkov and scintillation signals in head and neck radiotherapy. Phys. Med. Biol 64, 145021 (2019). [PubMed: 31146269]
21. Tendler II et al. Experimentally Observed Cherenkov Light Generation in the Eye During Radiotherapy. Int. J. Radiat. Oncol. • Biol. • Phys 0, (2019).
22. LaRochelle EPM, Shell JR, Gunn JR, Davis SC & Pogue BW Signal intensity analysis and optimization for in vivo imaging of Cherenkov and excited luminescence. Phys. Med. Biol 63, 085019 (2018). [PubMed: 29558363]
23. Steu S et al. A procedure for tissue freezing and processing applicable to both intra-operative frozen section diagnosis and tissue banking in surgical pathology. Virchows Arch. Int. J. Pathol 452, 305–312 (2008).
24. Reinhard E, Khan EA, Akyuz AO & Johnson G Color Imaging: Fundamentals and Applications. (CRC Press, 2008).
25. Gargesha M et al. Visualization of color anatomy and molecular fluorescence in whole-mouse cryo-imaging. Comput. Med. Imaging Graph. Off. J. Comput. Med. Imaging Soc 35, 195–205 (2011).
26. Ng CE, Keng PC & Sutherland RM Characterization of radiation sensitivity of human squamous carcinoma A431 cells. Br. J. Cancer 56, 301–307 (1987). [PubMed: 3663478]
27. Rock KL & Kono H The inflammatory response to cell death. Annu. Rev. Pathol 3, 99–126 (2008). [PubMed: 18039143]
28. Tesselaar E, Flejmer AM, Farnebo S & Dasu A Changes in skin microcirculation during radiation therapy for breast cancer. Acta Oncol. Stockh. Swed 56, 1072–1080 (2017).
29. Kaur RR, Kirby W & Maibach H Cutaneous allergic reactions to tattoo ink. J. Cosmet. Dermatol 8, 295–300 (2009). [PubMed: 19958434]
30. Schumann T, Peitsch WK, Géraud C, Goerdt S & Leverkus M Ultraviolet light tattoo complicated by granulomatous inflammation. J. Am. Acad. Dermatol 65, e124–e126 (2011). [PubMed: 21920233]
31. Tsang M et al. A visible response to an invisible tattoo. J. Cutan. Pathol 39, 877–880 (2012). [PubMed: 22905688]
32. Regensburger J et al. Tattoo inks contain polycyclic aromatic hydrocarbons that additionally generate deleterious singlet oxygen. Exp. Dermatol 19, e275–281 (2010). [PubMed: 20545755]

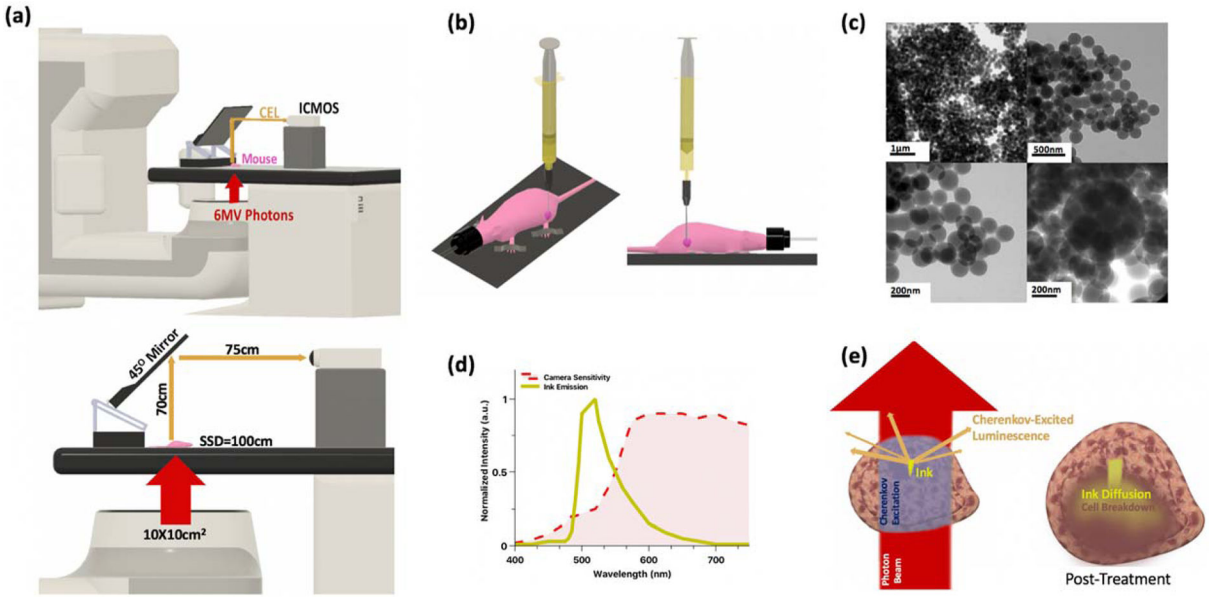

Figure 1 -

(a) Experimental imaging setup for *in vivo* measurements (models drawn to scale); room lights are off and entire system is covered under blackout curtain; **(b)** Intratumoral injection of mouse using stereotaxic platform (not shown) for consistent injection depth orthogonal to table in center of dark pink tumor (tumor not drawn to scale for illustrative purposes) with anesthetized mouse immobilized on the platform; **(c)** Tattoo ink (diluted 1:9 with ethanol) imaged using transmission electron microscopy, shown at various magnifications ranging from 17,000x to 26,000x magnification. Average particle size measured at 220nm. **(d)** Emission spectra of tattoo ink in solution (diluted 1:9 with ethanol) measured on spectrofluorometer with a 380nm excitation (shown in yellow) and the wavelength-dependent photocathode sensitivity (shown in red) (e) Close-up schematics of the injected tumor: left (pre-treatment, during initial image) - Cherenkov photons are generated where the tissue is irradiated by the beam (beam not drawn to scale for illustrative purposes), cherenkov photons excite the phosphorescent ink and delayed optical photons emit from within the tumor tissue to be detected by the ICMOS; right (post-treatment) – responsive tumor shows an expanded volume as tumor fills with inflammation in response to radiation-induced necrosis (shown in dark brown), the ink inclusion also expands in all directions as the ink breaks down with the tumor cell break down.

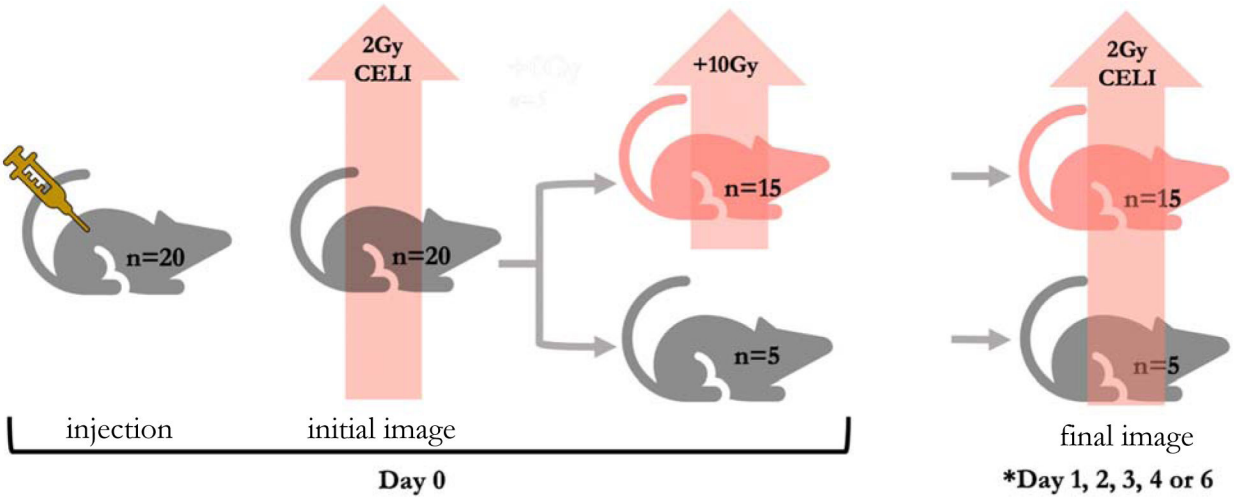

Figure 2 -

Workflow diagram of *in vivo* procedures/measurements for each mouse. All twenty mice received a 2Gy radiotherapy fraction on Day 0 for an initial CEL image immediately following the phosphorescent tattoo ink injection to measure the baseline spread of the ink. Fifteen mice received an additional 10Gy dose of radiation to the tumor. All twenty mice received a second 2Gy radiotherapy fraction for a final CEL image on a later day (*****refer to Table 2 for the number of mice re-imaged with CELI per day.)

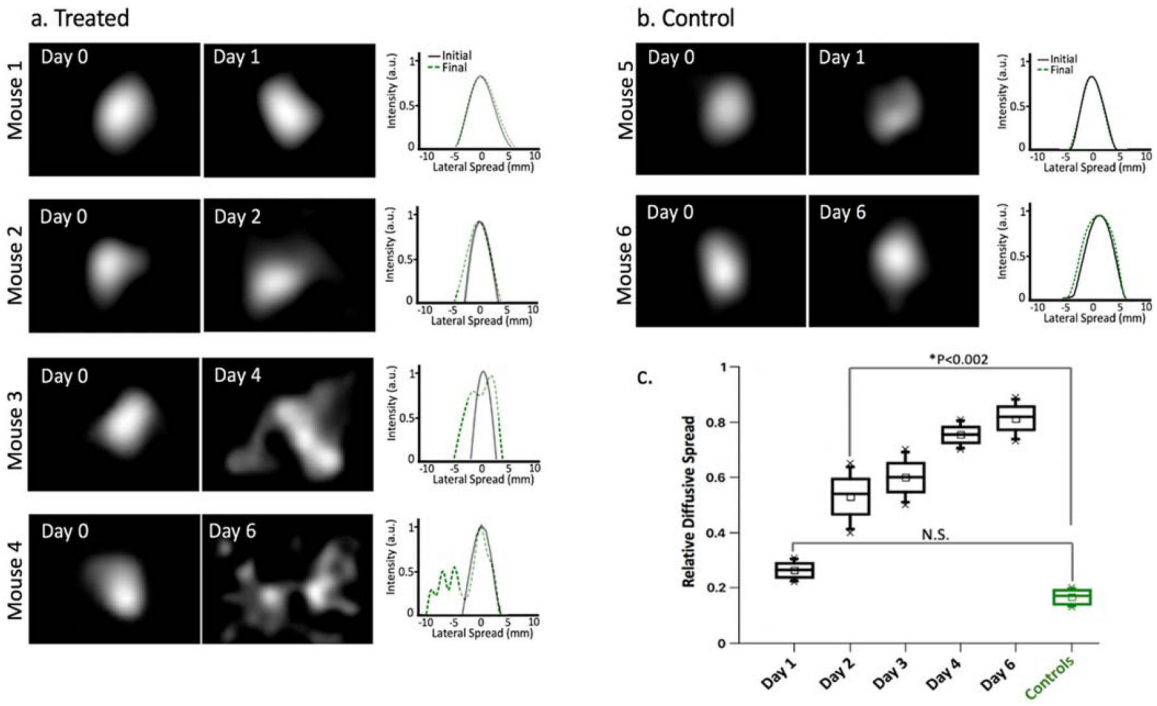

Figure 3-

In vivo Cherenkov-excited imaging of phosphorescent dye injected into mice with A431 tumors. (a) *In vivo* phosphorescent images of four treated mice on Day 0 (acquired immediately after injection) compared to the final diffusive ink spread (acquired immediately before sacrificing) with the corresponding intensity profile plots shown to the right. (b) *In vivo* phosphorescent ink images and intensity profile plots for two control mice. (c) Boxplots summarizing the relative change in diffusive spread measured in mice grouped by day post-treatment (calculated using the full width at 20% maximum of the Day 0 profile plot as the reference value); abbreviations: N.S. = not significant, ** p-value <0.002

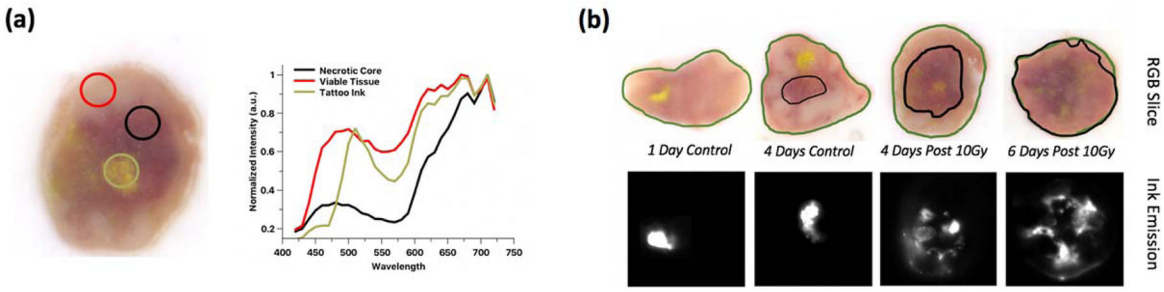

Figure 4-

Results of color detection algorithm from hyperspectral cryo-imaging data. **(a)** Regions of interest on treated tumor slice corresponding with reflectance spectra plots that were used to differentiate the non-perfusing necrotic core tissue **(b)** Results of the color detection algorithm based on part (a) input for example tumor slices.

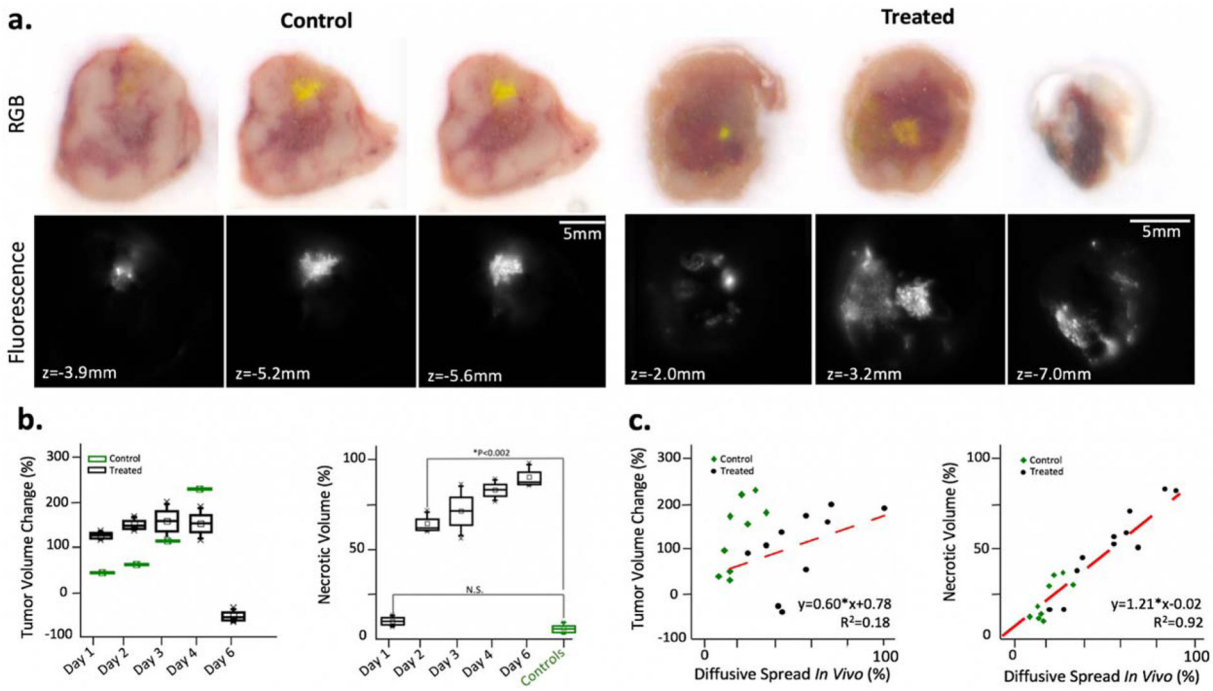

Figure 5 -

Ex vivo cryo-imaging of tumors from untreated and treated mice in 100μm slices. **(a)** RGB images and fluorescence images taken with a 470nm excitation and 560nm filter; slices presented for control and treated mouse each euthanized after 4 days post-injection. **(b)** boxplots of percentage change in tumor volume measurements from Day 0 to day of euthanasia and boxplots of percentage of necrotic tumor volume organized by day post-treatment or controls **(c)** plots of relative diffusive measured *in vivo* with percent tumor volume change and with percent necrotic volume; linear fits shown in red.

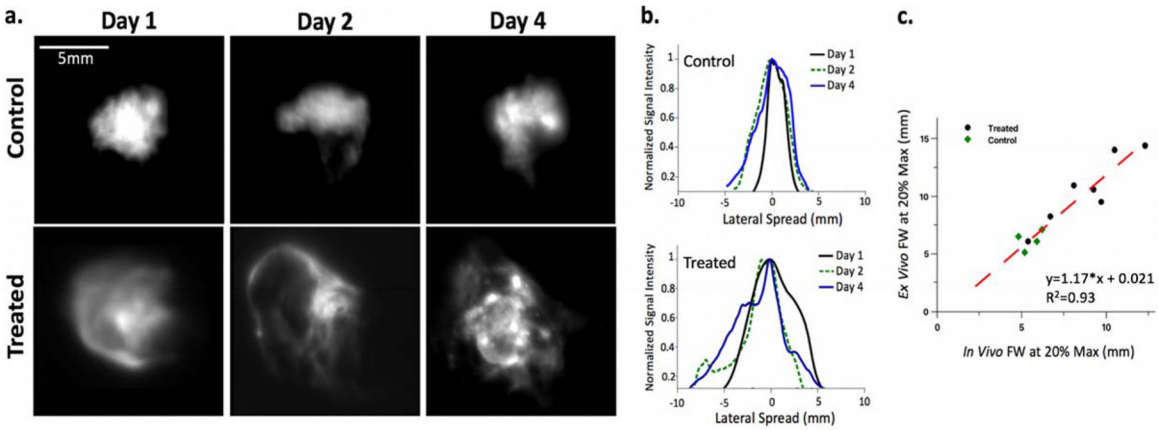

Figure 6 -

(a) Z-projections of ex vivo image stack for 3 control and 3 treated tumors after one two and four days post injection, (b) corresponding profile spreads and (c) Ink diffusion as measured by full width at 20% maximum value of profile spread plots using the final in vivo Cherenkov-excited acquisition compared with the Z-project of the ex vivo cryo-fluorescence slice imaging; linear fit shown in red with R^2=0.93.

Table 1:

Summary of Mice by Day of Second CELI Acquisition

Day of Second CEL Image	Treated (n)	Control (n)
Day 1	2	1
Day 2	2	1
Day 3	2	2
Day 4	2	2
Day 6	3	3
Total	**11**	**9**